Published OnlineFirst February 12, 2019; DOI: 10.1158/0008-5472.CAN-18-1604

Tumor Biology and Immunology

Cancer Research

Acidification of Tumor at Stromal Boundaries Drives Transcriptome Alterations Associated with Aggressive Phenotypes

Nazanin Rohani[1], Liangliang Hao[1,2], Maria S. Alexis[3], Brian A. Joughin[1,3,4], Konstantin Krismer[1,3,4,5], Mira N. Moufarrej[3], Anthony R. Soltis[3], Douglas A. Lauffenburger[3], Michael B. Yaffe[1,3,4,6,7], Christopher B. Burge[6], Sangeeta N. Bhatia[1,2,7,8,9], and Frank B. Gertler[1,6]

Abstract

Acidosis is a fundamental feature of the tumor microenvironment, which directly regulates tumor cell invasion by affecting immune cell function, clonal cell evolution, and drug resistance. Despite the important association of tumor microenvironment acidosis with tumor cell invasion, relatively little is known regarding which areas within a tumor are acidic and how acidosis influences gene expression to promote invasion. Here, we injected a labeled pH-responsive peptide to mark acidic regions within tumors. Surprisingly, acidic regions were not restricted to hypoxic areas and overlapped with highly proliferative, invasive regions at the tumor–stroma interface, which were marked by increased expression of matrix metalloproteinases and degradation of the basement membrane. RNA-seq analysis of cells exposed to low pH conditions revealed a general rewiring of the transcriptome that involved RNA splicing and enriched for targets of RNA binding proteins with specificity for AU-rich motifs. Alternative splicing of Mena and CD44, which play important isoform-specific roles in metastasis and drug resistance, respectively, was sensitive to histone acetylation status. Strikingly, this program of alternative splicing was reversed *in vitro* and *in vivo* through neutralization experiments that mitigated acidic conditions. These findings highlight a previously underappreciated role for localized acidification of tumor microenvironment in the expression of an alternative splicing-dependent tumor invasion program.

Significance: This study expands our understanding of acidosis within the tumor microenvironment and indicates that acidosis induces potentially therapeutically actionable changes to alternative splicing.

Introduction

Acidification of the microenvironment plays established roles in tumor progression, and provides a hostile milieu that advantages tumor cell survival and growth compared with noncancerous cells (1–3). Unlike normal cells, cancer cells can adapt to survive in low pH environments through increased glycolytic activity and expression of proton transporters that normalize intracellular pH. Acidosis-driven adaptation also triggers the emergence of aggressive tumor cell subpopulations that exhibit increased invasion, proliferation, and drug resistance (4–7). Acidosis also promotes immune escape, which maintains tumor growth (8).

How acidosis induces such phenotypes is only partially understood. The effects of extracellular acidity on cell invasion have been characterized mainly *in vitro* (9). For example, acidosis can modulate the subcellular localization and function of cytoskeletal regulatory proteins that underlie cell migration and invasion through protonation of critical pH-sensitive residues (10, 11). Extracellular acidification may also contribute to aggressive phenotypes through modulation of transcriptome dynamics. Transcriptome-wide studies suggest that tumor stressors such as hypoxia, nutrient starvation, and lactate acidosis can each regulate gene expression at the transcriptional and posttranscriptional levels *in vitro* (12–14). For instance, low extracellular pH induces increased histone deacetylation, thereby influencing the expression of certain stress responsive genes and concomitantly contributing to normalization of intracellular pH through the enhanced release of acetate anions that are co-exported with protons through monocarboxylate transporters (15, 16). However, how these changes influence transcriptome dynamics is not well understood, nor is it clear whether changes in gene expression arising from such stresses *in vitro* also correlate with those induced by equivalent physiologic stressors *in vivo*.

[1]Koch Institute for Integrative Cancer Research, MIT, Cambridge, Massachusetts. [2]Institute for Medical Engineering and Science, Massachusetts Institute of Technology, Cambridge, Massachusetts. [3]Department of Biological Engineering, MIT, Cambridge, Massachusetts. [4]Center for Precision Cancer Medicine, MIT, Cambridge, Massachusetts. [5]Computer Science and Artificial Intelligence Laboratory, MIT, Cambridge, Massachusetts. [6]Department of Biology, MIT, Cambridge, Massachusetts. [7]Department of Medicine, Brigham and Women's Hospital and Harvard Medical School, Boston, Massachusetts. [8]Broad Institute of Massachusetts Institute of Technology and Harvard, Cambridge, Massachusetts. [9]Howard Hughes Medical Institute, Cambridge, Massachusetts.

Note: Supplementary data for this article are available at Cancer Research Online (http://cancerres.aacrjournals.org/).

Corresponding Authors: Frank B. Gertler, Massachusetts Institute of Technology, 77 Massachusetts Avenue, 76-361a, Cambridge, MA 02139. Phone: 617-253-5511; Fax: 617-253-5511; E-mail: fgertler@mit.edu; and Nazanin Rohani, rohani.nazanin@gmail.com

doi: 10.1158/0008-5472.CAN-18-1604

Published OnlineFirst February 12, 2019; DOI: 10.1158/0008-5472.CAN-18-1604

Because of technical limitations, the spatial characteristics of acidic tumor tissue have been inferred mainly from bulk pH measurements (17, 18). Although these studies provide insights into the degree of acidification *in vivo* and highlight its heterogeneity, it has not been feasible to establish at cell-level resolution which areas within tumor microenvironment are acidic, nor has it been straightforward to determine how localized acidification correlates with molecular markers of cell invasion *in vivo*. Here we exploit the established ability of the pH low insertion peptide (pHLIP) to label cells exposed to acidic conditions *in vivo* (19, 20). pHLIP stably inserts into the membrane of cells exclusively under acidic conditions (<pH 6.5; ref. 19). We establish that pHLIP can be used to identify cells within acidic areas of the tumor at histologic resolution. We demonstrate that acidic areas extend beyond the hypoxic core of the tumor and that the invasive fronts at the tumor–stroma interface are acidic *in vivo*. Using RNA-seq analyses of mouse and human mammary carcinoma cell lines in response to low pH *in vitro*, we find that acidosis widely modulates RNA splicing and enriches for targets of specific types of RNA binding proteins. The pH-responsive expression of a set of functionally relevant splice variants from this signature was validated *in vivo* and *in vitro* and the splicing of two of these events was sensitive to changes in histone acetylation. Our study highlights the underappreciated impact of extracellular acidification as a critical feature of the tumor microenvironment that locally influences transcriptome dynamics to promote the acquisition of invasive phenotypes.

Materials and Methods

Immunofluorescence and image analysis

Tumor tissue sections were stained and processed as previously described (21). In short, tumor tissue was excised from mice and fixed in 10% buffered formalin and embedded in paraffin. Tumors from MMTV-PyMT mice were fixed in 10% buffered formalin and embedded in paraffin. Sections from FFPE human breast cancer tumors were obtained from Metastat Inc. Tissue sections (5 μm thick) were deparaffinized followed by antigen retrieval using Citra Plus solution (Biogenex). Sections were blocked with serum and incubated with primary antibodies overnight at 4°C. Fluorescently labeled secondary antibodies were added at room temperature for 2 hours. Images were collected using a DeltaVision microscope with plan-apo 20× objective 1.4NA and CoolSNAP HQ camera (Photometrics), controlled by softWoRx software (GE Healthcare). Eight to 10 images at 0.2 μm steps were collected, deconvolved, and 2D-projected for maximum signal intensity. Exon-specific probe were custom designed for CD44 E19 and RNAscope 2.5 HD assay was performed according to manufacturer guidelines and detected by Red Kit (catalog no. 322360). Following RNAscope protocol completion antibody labeling and immunofluorescence staining was performed. The images were then subjected to contrast adjustments using ImageJ and quantified for the percentage of overlap between markers in red and green channels using InForm software (Perkin Elmer). Image quantification workflow consists of tissue segmentation to segment tumor and nontumor regions followed by cell segmentation using DAPI counterstain using built-in algorithms. The images were then scored using a thresholding approach for double positivity or degree of positivity. Cells-based segmentation data, including positional information relative to tumor edge and degree of positivity generated in the above analysis was used to identify 3+ positive cells and localization relative to tumor edge. Image segmentation and analysis was performed on at least three tumors from four different mice and three to five areas per tumor. To keep thresholding and other criteria consistent across analyzed groups, image analysis was performed for each experiment with all images as a batch. Antibodies used in the study are listed in Supplementary Table S1.

RNA isolation and RT-qPCR validations

Total RNA from cell lines was extracted using RNeasy Plus Mini Kit (Qiagen). RNA from tumor tissues was extracted in Trizol and homogenized with a Bullet Blender (Next Advance) according to the manufacturer's instructions. One to 100 ng of RNA was reverse transcribed with SuperScript III (Invitrogen). The resulting cDNAs were used for qPCR analysis using iQ SYBR Green Supermix (BioRad) in triplicates. qPCR and data collection were performed on a StepOne system (Applied Biosystems). Primers used for qPCR analysis are listed in Supplementary Table S2. Data were analyzed according to $\log_2$-fold change ΔΔCt method using GAPDH as a reference gene.

Illumina sequencing

Raw and processed RNA-seq data can be found at Gene expression ominibus, NCBI, accession number: GSE119646. See Supplementary Materials and Methods for detailed methods.

Bioinformatics analysis

Gene set enrichment and network visualization. Gene set enrichment analyses (GSEA) were performed on ranked lists of genes that were generated using mean $\log_2$- fold change of all commonly expressed genes in both mouse and human datasets. Pre-ranked GSEA analysis was performed using the GSEA software available from the Broad Institute (http://www.broadinstitute.org/gsea/index.jsp; ref. 22). Gene sets significantly associated with transcript level up- or downregulation by low pH ($P < 0.05$ and FDR < 0.01) were then represented in enrichment networks wherein nodes correspond to significantly-enriched GO terms, and edges indicate pairs of gene sets that share genes. Node sizes correspond to the number of genes in the GO term gene sets that also occur in the gene input list. Edge weights correspond to the overlap coefficients between pairwise GO term gene set comparisons. Two gene sets A and B have an overlap coefficient equal to $|A \cup B|/\min(|A|,|B|)$, where $|X|$ represents the number of genes in gene set X. GSEA results were processed using custom scripts written in MATLAB to generate graphml files with the properties described above. The resultant networks were arranged using a combination of manual positioning and automated layout functions in the yEd Graph Editor (yWorks GmBH, Tübingen, Germany). Related ontological terms were grouped using a natural clustering algorithm that relies on the edge betweenness clustering method. Nodes were re-colored to reflect the cluster in question, and networks of related ontologies were manually assigned a group label to represent shared high-level biological processes across all nodes.

Spectrum motif analysis

We used the spectrum motif analysis (SPMA) approach from Transite (https://transite.mit.edu; ref. 23) to identify RNA binding proteins whose target transcripts are upregulated in low pH conditions. The original list of transcripts was sorted by the

Published OnlineFirst February 12, 2019; DOI: 10.1158/0008-5472.CAN-18-1604

$\log_2$-fold change between the low pH and physiologic pH conditions in ascending order, subdivided into 40 bins and RBP motif enrichment was calculated for each bin with respect to the entire list of transcripts. Significance levels are indicated by one, two, or three asterisks (*P*-value less than or equal to 0.05, 0.01, and 0.001, respectively) and refer to the putative binding site enrichment values per bin. A linear model was fit to the 40 enrichment values describing the relationship between fold change and number of putative binding sites. Goodness of fit was measured by adjusted R^2. Additionally, local consistency scores (CS; ref. 23) were used to identify nonrandom arrangements of putative binding sites across the spectrum of fold change sorted transcripts. The Transite source code is hosted on GitHub (https://github.com/kkrismer/transite).

CLIP and RNA-seq overlap analysis

CLIP datasets were taken from the ENCODE project (eCLIP datasets available at encodeproject.org, accession numbers: TIA1: ENCSR623VEQ and ENCSR333PZV; KHDRBS1: ENCSR628IDK and ENCSR197NFH) and from (GEO accession number GSE29943 for HITS-CLIP of HuR; refs. 24, 25). Metaplots of CLIP densities in 3′UTRs were plotted separately for three categories of genes: (i) up in pH6, where gene expression was increased at least 1.5-fold in pH6 relative to pH7; (ii) down in pH6, where gene expression was decreased at least 1.5-fold in pH6 relative to pH7; (iii) control, where the fold-change in gene expression was less than 1.1-fold between both conditions. For each 3′UTR, we assessed the CLIP peak height (peak enrichment over input control) across 200 evenly sized-windows that spanned the whole UTR (i.e., window size is UTR length/200). Metaplots were then, generated by averaging CLIP peak densities across all genes in each window. Significance was assessed in each window by the Kolmogorov–Smirnov test.

In vivo mouse experiments

All experiments were performed according to the Guide for the Care and Use of Laboratory Animals and were approved by the National Institutes of Health, and the Committee on Animal Care at the Massachusetts Institute of Technology (Cambridge, MA). For sodium bicarbonate water therapy experiment, female MMTV-PyMT mice were obtained from Jackson laboratories at 4 weeks of age. Five to eight mice per group were randomized, before the emergence of palpable tumor, into control and bicarbonate water treated groups as described (26, 27). In summary regular or 200 mmol/L sodium bicarbonate water (equal to ~3.2 g/kg/day) was provided ad libitum for 8 weeks. For xenograft experiments, 2×10^6 MDAMB231 cells in 20% collagen 1 in PBS were injected into the fourth mammary fat pad of 6-week-old female NOD/SCID mice. Mice were similarly randomized in two groups of four mice each and the experiment was carried out for 8 weeks postinjection. Upon completion of the experiment, mice were subjected to tail-vein injection of 100 μL of 40 μmol/L Cy7 labeled pHLIP peptide [N→C: AC(Cy7)DDQNPWRAYLDLLF-PTDTLLLDLLW-DLys-DLys synthesized by CPC Scientific, Inc.] 6 to 12 hours prior to sacrifice. For the detection of hypoxic areas of the tumor, 1 hour prior to sacrifice 60 mg/kg hypoxyprobe was injected intraperitoneally according to manufacturer instructions. The pHLIP-Cy7 intensity for localization and distribution in nonfixed fresh tumors and major organs was imaged immediately after scarification of mice using a near-infrared florescent imaging system (Odyssey CLX, LI-COR Biosciences). Next, tumor and lungs were either fixed in 10% formalin for histological analysis, followed by Cy7 antibody detection, or snap frozen for further RNA extraction or dissociated for FACS sorting.

FACS sorting

Tumors were collected from PyMT mice injected with Cy7-pHLIP, and tumors were then minced with a razor blade into pieces <1 cm, and the minced chunks were then rinsed three times with PBS and then digested with collagenase. Digested tissues were then dissociated into single cell suspensions by 4× passing through 18G followed by 19G needles. The dissociated tumor cells were then washed twice with DMEM with 10% FBS and then filtered through 70 and 40 μm cell strainers and pelleted. The cell pellets were then resuspended into 10% FBS in PBS for FACS sorting. pHLIP-labeled Cy7 positive cells and negative populations were sorted using the 640 nm laser on a FACSAria cell sorter using the APC-Cy7 detector. Gating was determined using dissociated tumor cells from un-injected control mice.

Cell culture

Please see Supplementary Materials and Methods for information on cell lines and culture conditions. All cells were tested for mycoplasma using Lonza MycoAlert Mycoplasma Detection Kit in 2015 and 2017 and used for experiments at passage 3 to 5. MDA-MB-231 and 4T1 cell lines were obtained from ATCC and authenticated by ATCC using STR DNA profiling analysis method. LM2, SUM159, PyMT cell line and patient-derived PDX line were only authenticated using morphology check by microscope method. For the alteration of the pH conditions in the medium for each cell line, the sodium bicarbonate concentration was adjusted based on the Henderson–Hasselbalch equation in the base medium to reach pH 6.4 or 7.4. Medium was equilibrated at 37°C and 5% CO_2 for at least 12 hours prior to use. Cells were cultured at subconfluent density at normal (7.4) or low pH (6.4) for indicated time points in Supplementary Fig. S5 or 48 hours all other experiments. Hypoxia conditions were generated using hypoxic chamber at 0.2% oxygen, cells were cultured for 3 or 10 days in hypoxic chambers. Lactate acidosis was induced over 4 to 8 days by the addition of 5 mmol/L metformin to the medium. In both conditions, 50 mmol/L HEPES was added or eliminated to monitor the effect of buffering capacities. The pH and lactate-to-glucose ratio were measured from the media samples collected from each condition at the beginnings and ends of each experiment, using pH stripes and YSI bio analyzer for enzymatic measurement of glucose and lactate levels. HDAC inhibition experiment was performed by addition of 500 nmol/L Trichostatin A (Sigma T1952) or DMSO to cells cultured either in pH 6.4 or 7.4 conditions. Cells were lysed for protein or RNA extraction after 48 hours of culture.

Statistical analysis

The Student *t* test was used for paired data, and data are presented as means with SD. The *P*-value for significance of co-occurrence of two histologic markers is calculated from counts of cells with either marker, both, or neither using a one-tailed Fisher exact test, and odds ratios are calculated as the ratio of frequencies of a marker appearing in concert with a second marker vs. in the absence of the second marker. Hypergeometric statistics was used to identify significance of overlap in the bioinformatics analysis of mouse and human RNA-seq datasets.

Published OnlineFirst February 12, 2019; DOI: 10.1158/0008-5472.CAN-18-1604

Results

Tumor–stroma interface is acidic

To identify cells within the tumor microenvironment exposed to low extracellular pH, we used the pHLIP peptide to label acidic tumor regions *in vivo* prior to sacrifice. Fluorescently labeled pHLIP peptide was injected intravenously into either tumor bearing transgenic MMTV-PyMT mice or NOD/SCID immune compromised mice with orthotopically implanted MDA-MB-231 xenograft tumors. As expected, pHLIP was detected in the tumors collected from these mice, but was undetectable in healthy organs aside from kidney and liver, where the peptide is cleared from the body (Supplementary Fig. S1A and S1B; refs. 20, 28). Cy7-pHLIP-labeled cell areas were detected both in the unfixed bulk tissue using an NIR imager and in tumor cross sections using an antibody specific to Cy7 (Supplementary Fig. S1A′ and S1B′). To control for pHLIP labeling specificity, we analyzed alkalinized tumor samples taken from mice treated with bicarbonate drinking water. Neutralization of tumor acidity significantly reduced pHLIP labeling compared to controls (Supplementary Fig. S1A and S1B), confirming that pHLIP retention at the membrane requires an acidic tumor microenvironment *in vivo*.

We next examined the distribution of pHLIP retention within tumors. Images of stained tumor cross sections from mice injected with the pHLIP probe were analyzed using a cell-based segmentation approach. Thresholding of signal intensity was used to stratify cells based on pHLIP retention (Supplementary Fig. S1C–S1C′). Cells with the strongest pHLIP positivity were enriched at tumor–stroma interfaces both within primary tumors and in metastatic lesions in the lung (Fig. 1A and B), indicating that the tumor–stroma interface was acidic.

To confirm that pHLIP reliably labeled acidic tumor areas, we evaluated its overlap relative to two additional markers associated with low extracellular pH: expression of CA9 and of plasma membrane-localized LAMP2 (PM-LAMP2; refs. 2, 29, 30). CA9 is a major transporter that contributes to extracellular acidification through reversible hydration of carbon dioxide to bicarbonate and protons. CA9 expression significantly correlated with areas of pHLIP retention at cell membranes in both the primary tumor (Fig. 1C) and metastatic lesions (Supplementary Fig. S1D). Given the extensive overlap with, and similar patterns of CA9 expression (Fig. 1D; Supplementary Fig. S1E) relative to pHLIP positive cells in the mouse model, we used CA9 as a surrogate to label cells in acidic areas in human tumor tissues. Similar to the mouse tumors, the CA9 was enriched at tumor-stroma interfaces in human tumors (Supplementary Fig. S1F).

PM-LAMP2 indicates cellular adaptation to chronic acidosis (2, 31). PM-LAMP2 overlapped significantly with pHLIP labeled cells (Supplementary Fig. S2A) and most cells with PM-LAMP2 were proximal to the tumor–stroma interface confirming that it is acidic (Supplementary Fig. S2B). Similarly, in human IDC tumors, cells expressing CA9 significantly overlapped with cells exhibiting PM-LAMP2 (Supplementary Fig. S2C and S2D). Therefore, areas containing pHLIP labeled cells or cells expressing high levels of CA9 likely correspond to cellular areas exposed to acidic conditions *in vivo*.

Tumor acidification is widely assumed to be mainly co-incident with hypoxia, however, bulk level O_2 and pH measurements *in vivo* have demonstrated some level of discrepancy (17), indicating that well-oxygenated areas of the tumor may also be acidic. We compared the distribution of cells within hypoxic areas, marked by pimonidazol, relative to that of pHLIP labeled cells (Fig. 1E). Most hypoxic areas were acidic as expected, however, surprisingly, large populations of cells that were labeled by pHLIP were not hypoxic (Fig. 1E). Hypoxic areas labeled by piminidazole were mostly enriched at areas distant from the tumor–stroma interface (Fig. 1F). The low level of overlap between the two markers was not a consequence of incomplete pHLIP peptide perfusion into tissue as labeling of endothelial cells by CD31 revealed that pHLIP localized both in highly vascularized areas at the tumor rim (Supplementary Fig. S2E–S2E′) and in poorly vascularized areas at the tumor core (Supplementary Fig. S2E–S2E″).

Increased aerobic glycolysis, a characteristic of invasive cancer cells, contributes to acidification of tumor microenvironment. LDHA expression drives aerobic glycolysis through increased lactate and proton production, thus its expression is a molecular indicator for increased aerobic glycolysis (20, 29, 32, 33). We found that the majority of LDHA-positive cells were also labeled by pHLIP (Fig. 1G). In addition, similar to pHLIP, the distributions of LDHA and CA9 positive cells were highly enriched at tumor–stroma interfaces (Fig. 1H). Together, these findings suggest that pHLIP marks cellular areas within the tumor–stroma interface that are acidic but not necessarily hypoxic and that increased glycolytic metabolism may be a primary cause of extracellular acidity at the tumor–stroma interface.

Hallmarks of cell invasion and proliferation are enriched at acidic fronts

Although acidosis is associated with malignant progression and invasion, direct cell-level spatial correlations between regional acidity and molecular markers for invasion have not been demonstrated *in vivo*. We asked whether the acidic areas of the tumor exhibited features characteristic of invasive phenotypes. Most cells within acidic tumor areas marked by pHLIP in mouse or CA9 expression in human tumors also expressed high levels of the matrix metalloproteases MMP9 or MMP14, respectively (Fig. 2A; Supplementary Fig. S3A). In addition, cells with the highest levels of MMP9 or MMP14 expression were located closest to tumor–stroma interfaces (Fig. 2B; Supplementary Fig. S3B). Interestingly, as indicated by the absence of laminin staining, basement membranes were almost entirely disrupted adjacent to cellular areas that retained pHLIP at the membranes or that expressed CA9 (Fig. 2C; Supplementary Fig. S3C). Together, these observations suggested that the acidic areas are invasive tumor fronts.

In addition to promoting invasion, acidification is also thought to promote local tumor growth (6, 7). Consistent with this, we observed that 85% of Ki-67 positive cells were also labeled by pHLIP in MMTV-PyMT tumors (Fig. 2D). In human tumors, however, the overlap between CA9 and Ki-67 was lower but significant, with 36% of CA9 positive cells also positive for Ki-67 expression (Supplementary Fig. S3D). Nevertheless, most Ki-67 positive cells were localized to the tumor-stroma interface in both mouse and human (Fig. 2E; Supplementary Fig. S3E). This pattern was similarly observed in lung metastatic lesions (Fig. 2F and G), suggesting that the cells within the acidic front are proliferative. Together, these data demonstrate that the low-pH areas of the tumor are enriched for cells that are invasive and proliferative.

Acidosis modulates gene expression and splicing

Although it is known that low extracellular pH elicits aggressive tumor cell phenotypes such as increased MMP activity, migration and invasion (34, 35), the extent to which local extracellular

Published OnlineFirst February 12, 2019; DOI: 10.1158/0008-5472.CAN-18-1604

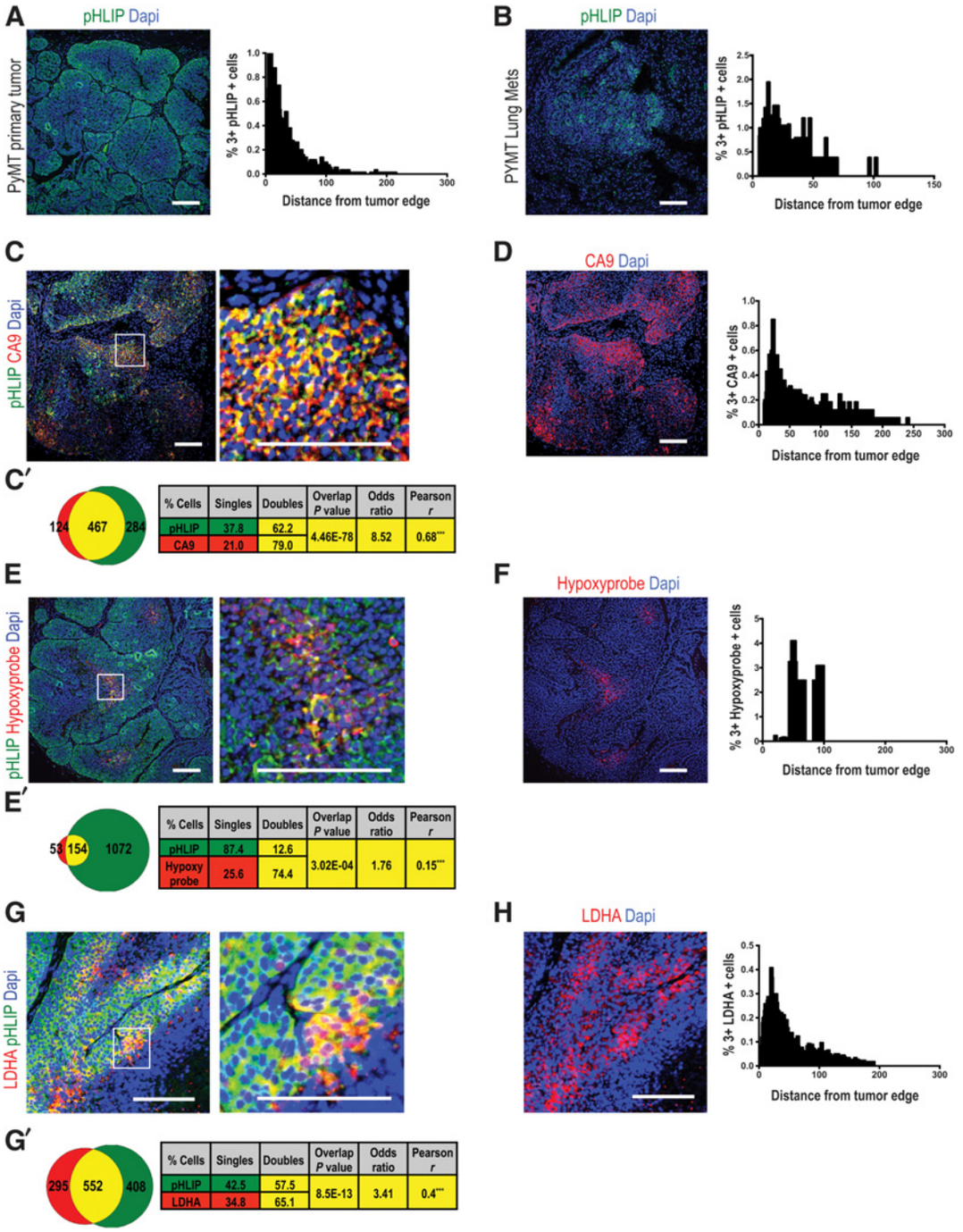

Figure 1.

Tumor–stroma interface is acidic. **A** and **B,** Immunofluorescence detection of pHLIP-Cy7 in primary tumors (**A**) and metastatic lesions (**B**) from PyMT mice. Graphs show localization of pHLIP positive cells relative to tumor dimensions. *x*-axis, distance in pixels from tumor edge; *y*-axis, mean percentage of (3+) cells (highest levels of pHLIP membrane positivity). **C,** Carbonic anhydrase (CA9)–expressing cells overlap cells with pHLIP-labeled membranes. **D,** Spatial distribution of CA9-positive cells within the tumor. Highest expressing cells located proximal to the tumor–stroma interface. **E,** Degree of overlap between acidic and hypoxic areas. Cell-based colocalization analysis for images costained to detect hypoxic areas using piminidazol and acidic areas in tumors collected from mice injected with both probes. **F,** Spatial distribution of hypoxic areas relative to the tumor–stroma interface. **G,** Immunofluorescence labeling for LDHA and pHLIP. **H,** The spatial distribution of LDHA-positive cells. **C′, E′,** and **G′,** Summary of cell-based segmentation and colocalization analyses. Venn diagrams show average cell numbers. Tables show the percentage of single- and double-positive cells for each marker. *P* value and odds ratio indicate significance and degree of association for the two marker. Pearson *r* measures degree of cell-wise intensity correlation across samples. Pearson *P* values were quantified using two-tailed Student *t* test. ***, $P \leq 0.001$. Scale bars, 100 μm.

Published OnlineFirst February 12, 2019; DOI: 10.1158/0008-5472.CAN-18-1604

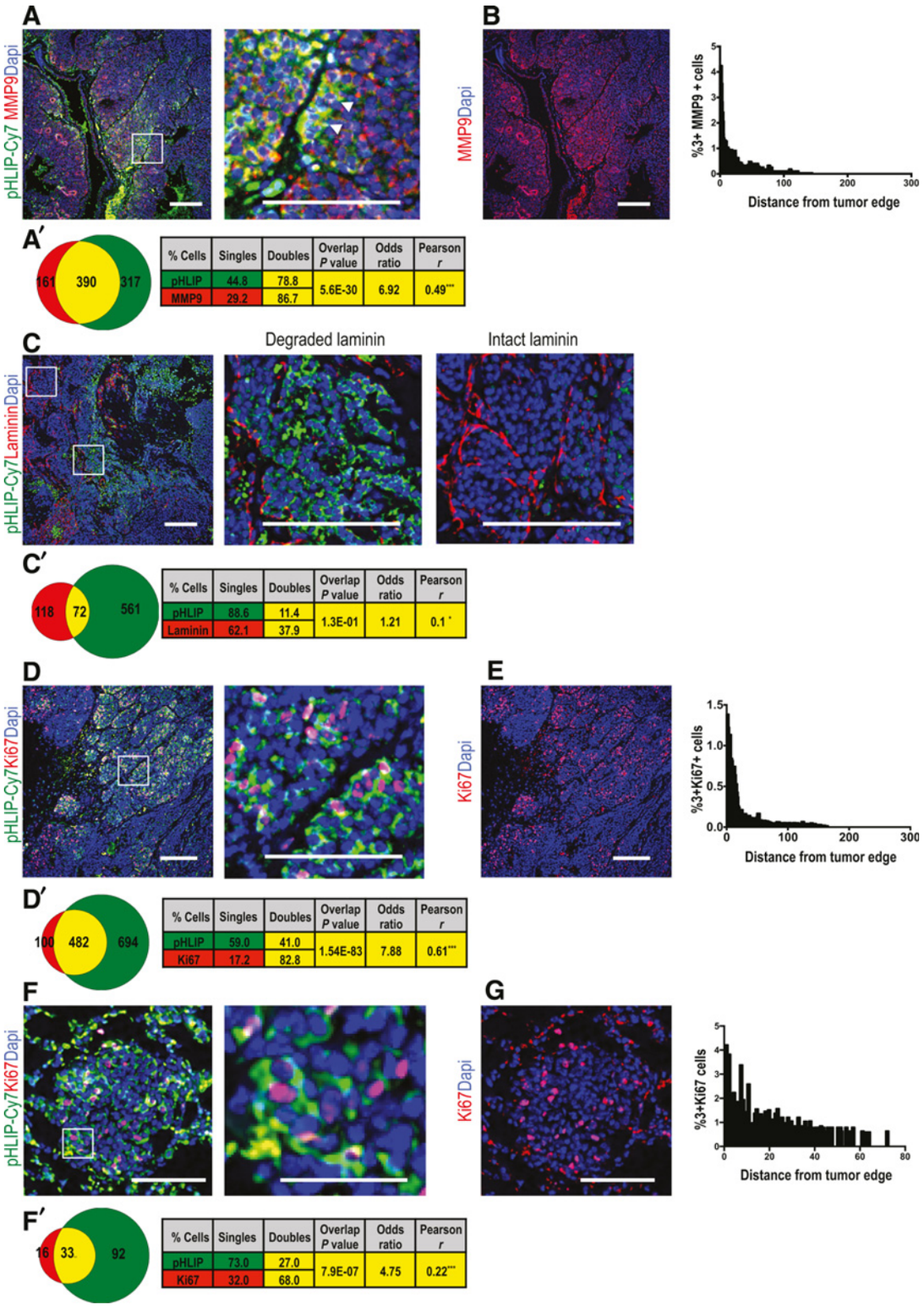

Figure 2.

Acidic front is invasive and proliferative. **A,** Immunofluorescence labeling of PyMT tumor tissues for MMP9 and pHLIP. **A′,** Cell-based overlap and signal intensity correlation of MMP9 and pHLIP. **B,** MMP9 distribution relative to tumor dimension. **C,** Laminin is absent from cells that are pHLIP-positive. **C′,** Cell-based analysis of laminin (basement membrane) relative to acidic areas marked by pHLIP. **D** and **F,** Immunofluoresnce of Ki-67 and pHLIP in primary tumor (**D**) and in metastatic lesions of the lung (**F**). **D′** and **F′,** Cell-based overlap and signal intensity correlation of pHLIP and Ki-67. **E–G,** Ki67-positive cells were enriched at the tumor–stroma interface. Pearson *P* values were quantified using two-tailed Student *t* test (*, $P \leq 0.05$; ***, $P \leq 0.001$). Scale bars, 100 μm.

Published OnlineFirst February 12, 2019; DOI: 10.1158/0008-5472.CAN-18-1604

acidification triggers changes in gene expression is less well studied. We performed RNA-seq analyses of MDA-MB-231, a human TNBC breast cancer cell line, and 4T1, a mouse mammary carcinoma cell line, cultured under either physiologic (pH 7.4) or low pH (pH 6.4) conditions induced by modification of the concentration of sodium bicarbonate. We observed concordant, pH-dependent changes in expression of 2752 genes in the mouse and human cell lines (Fig. 3A). Gene set enrichment analysis (GSEA) of the transcriptomic changes common to both mouse and human was used to identify the biological processes most affected by acidification. Network analysis of gene sets with an FDR < 0.01 that associated with genes up- or downregulated in both species under acidic conditions revealed a large number of changes associated with RNA processing and RNA splicing (Fig. 3A′). Other less pronounced gene sets included regulation of GTPases, cell migration, immune response, oxidative phosphorylation, and mechanisms associated with cell response to stress. This finding highlighted the possible effect of tumor acidosis on posttranscriptional regulation of gene expression.

An assessment of exon usage in both mouse and human revealed a global rewiring of splicing under low pH. The density plot for percent spliced in (PSI) values in low or normal pH indicates that acidosis deregulated RNA splicing, and in particular, it affected the splicing of constitutive exons PSI = 0 or 1 (Fig. 3B). Therefore, acidosis induces a rewiring of transcriptome, leading to the emergence of alternatively spliced isoforms and deregulating inclusion or exclusion of constitutive exons. In addition, and similar to previous reports for hypoxia (12), a survey of different types of splicing events indicated that low pH conditions gave rise to larger numbers of retained introns (Supplementary Fig. S4A). To identify the biological processes affected by alternative splicing under acidosis, we performed GSEA analysis focused on orthologous exons altered in both the mouse and human datasets in response to low pH. As expected, most significant gene sets enriched in the splicing signature were associated with RNA interactions, such as genes encoding splicing factors and RNA binding proteins that are known to be heavily dependent on autoregulation by alternative splicing (Fig. 3B). Other genes exhibiting significant changes in splicing patterns were associated with cytoskeleton. Pathway analysis of these events suggested that the splicing events could be associated with genes involved in regulation of spliceosome machinery and in regulation of cell adhesion, respectively (Fig. 3B′–B″). These results suggest that low extracellular pH can trigger RNA splicing-mediated changes in cytoskeletal machinery, which may contribute to acidosis-induced cell invasion.

Targets of RNA binding proteins that interact with AU-rich motifs are enriched in low pH transcriptomic signature

Given the major impact on the global deregulation of constitutive exons and changes in splicing patterns, we asked if a specific set of RNA binding proteins contributes to the global rewiring of the transcriptome in response to extracellular acidity. We took advantage of publicly available datasets to investigate how RBP targets are distributed across pH-induced transcriptomic changes in mouse and human, applying the "SPMA" approach from Transite, a novel bioinformatics platform (23). SPMA identified RBPs whose putative target transcripts were arranged in a nonrandom fashion across the sorted list of pH induced transcripts organized by their $\log_2$-fold change. Most strikingly, putative binding sites of the ELAVL/HUR family of RNA binding proteins were highly enriched in transcripts up regulated in low pH. Moreover, there was a clear linear relationship between fold change and enrichment of putative ELAVL/HUR binding sites, as measured by adjusted R^2 values of the fitted linear models (0.769 for human and 0.732 for mouse) and highly significant local consistency scores with P values of 2×10^{-7} and 4×10^{-7} for human and mouse, respectively (Supplementary Table S3; Fig. 4A). An overlap of RBPs whose putative binding sites were most significantly enriched in both RNA-seq datasets revealed a consistent enrichment of AU-rich motifs in transcripts that were upregulated in low pH (Fig. 4B).

To strengthen this observation, we investigated the publicly available CLIP dataset and its overlap with our RNA-seq data. We found significantly greater CLIP peak densities for HUR, TIA1, and KHSRP around the 3′-UTR regions of genes upregulated in response to low pH relative to control (Fig. 4C). This alternative bioinformatics approach confirmed that RBPs with preferential binding to AU-rich motifs were enriched in genes upregulated in low pH. These RBP families are mostly known for their effect on RNA stability, but some also play important roles in RNA splicing. Members of the ELAVL family, for instance, under stress conditions shuttle to cytoplasm to stabilize stress-sensitive transcripts and promote cell survival (36). This finding suggests a potential role for RBPs that interact with AU-rich motifs, and in particular ELAVL/HUR in modulating the pH-induced gene expression changes. Whether or not ELAVL and other AU-rich motif-binding RBPs influence the significant changes in RNA splicing, isoform-specific mRNA stabilization or both requires further investigation.

Extracellular acidity is necessary and sufficient for the induction of candidate splicing events

To validate our bioinformatics analysis of acidosis induced alternative splicing, we selected candidate-splicing events from genes showing substantial pH-dependent changes informed by their known functional importance in the induction of aggressive tumor phenotypes (Supplementary Fig. S4B and S4C): (i) the inclusion of exon19 of CD44, involved in drug resistance (37, 38); (ii) the inclusion of exon 4 (INV) of Mena (ENAH), also known as $Mena^{INV}$, an isoform that promotes cell invasion and metastasis (39, 40); (iii) the exclusions of exon 23 in DOCK7 with a potential role in regulating cytoskeletal dynamics; (iv) the exclusion of exon6 in DLG1, with a potential role cell polarity (41, 42). With the exception of exon 19 of CD44, all selected events were common to both mouse and human pH-dependent responses. We first validated the reproducibility of these pH-responsive splicing events across a panel of human breast cancer lines including MDA-MB-231 and its metastatic derivative LM2, and SUM159 as well as a cell line derived from a PDX model for a triple-negative mammary carcinoma patient (43). In parallel, the conserved events in these genes were assessed in 4T1 cells as well as in a cell line derived from an MMTV-PyMT tumor. RT-qPCR analysis indicated that all observed pH-dependent changes in these candidates were reproducible in all cell lines examined (Supplementary Fig. S4D).

We then investigated whether these events were directly responsive to extracellular pH alteration. First, we asked if the events were induced as an immediate response to extracellular acidification or were a consequence of adaptation. MDA-MB-231 cells were cultured for 4, 12, 16, 48, and 96 hours prior to analysis. Except for CD44, which showed apparent inclusion of the exon as early as

Published OnlineFirst February 12, 2019; DOI: 10.1158/0008-5472.CAN-18-1604

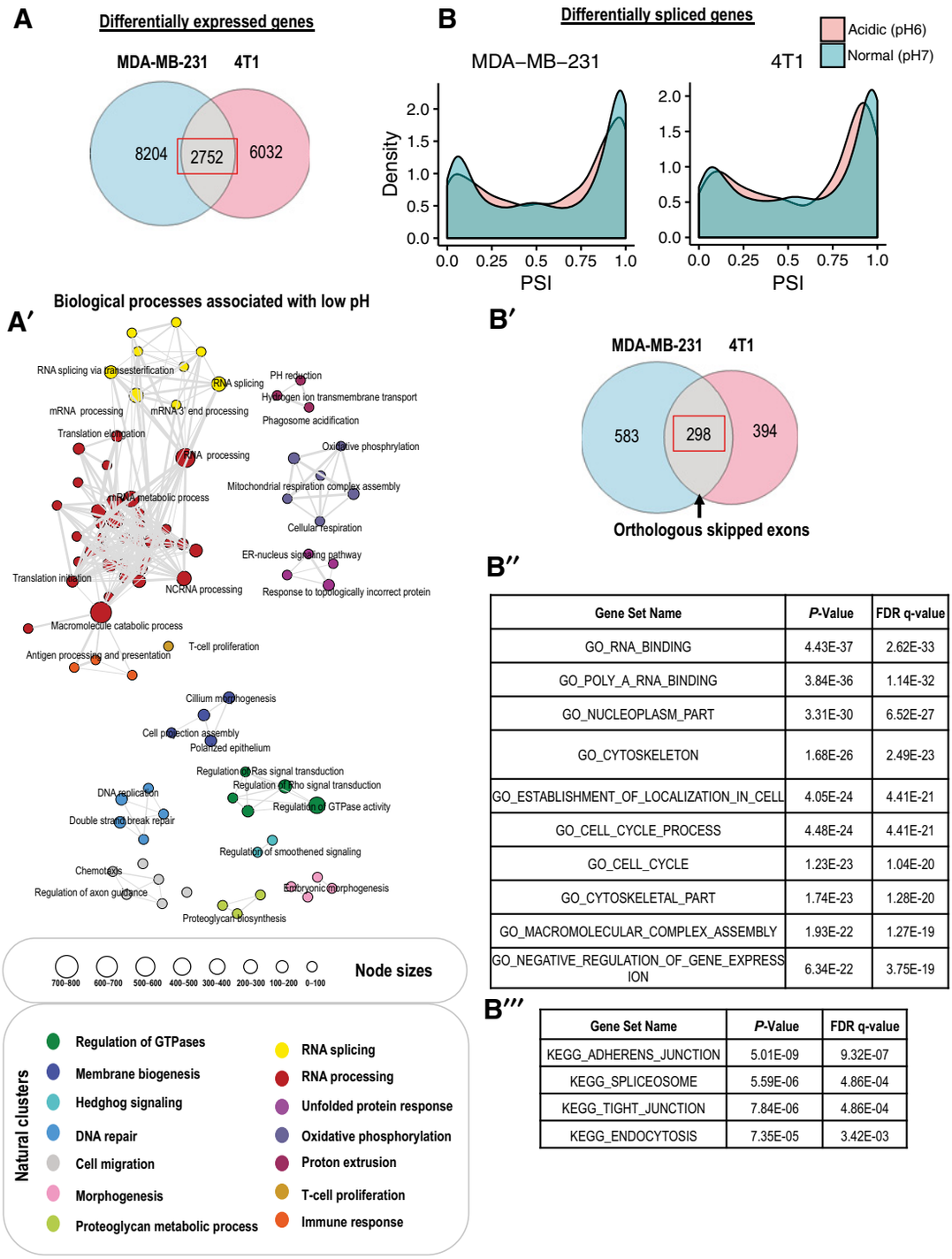

Gene Set Name	*P*-Value	FDR q-value
GO_RNA_BINDING	4.43E-37	2.62E-33
GO_POLY_A_RNA_BINDING	3.84E-36	1.14E-32
GO_NUCLEOPLASM_PART	3.31E-30	6.52E-27
GO_CYTOSKELETON	1.68E-26	2.49E-23
GO_ESTABLISHMENT_OF_LOCALIZATION_IN_CELL	4.05E-24	4.41E-21
GO_CELL_CYCLE_PROCESS	4.48E-24	4.41E-21
GO_CELL_CYCLE	1.23E-23	1.04E-20
GO_CYTOSKELETAL_PART	1.74E-23	1.28E-20
GO_MACROMOLECULAR_COMPLEX_ASSEMBLY	1.93E-22	1.27E-19
GO_NEGATIVE_REGULATION_OF_GENE_EXPRESSION	6.34E-22	3.75E-19

Gene Set Name	*P*-Value	FDR q-value
KEGG_ADHERENS_JUNCTION	5.01E-09	9.32E-07
KEGG_SPLICEOSOME	5.59E-06	4.86E-04
KEGG_TIGHT_JUNCTION	7.84E-06	4.86E-04
KEGG_ENDOCYTOSIS	7.35E-05	3.42E-03

Figure 3.

Transcriptomic alterations in response to low extracellular pH. **A,** The expression of 2,752 genes (padj < 0.05, $\log_2$-fold change >0.5, mean control read count >10) in MDA-MB-231 and 4T1 cells significantly overlap (hypergeometric statistics, $P = 10^{-419}$). **A′,** The overlapping genes, ranked by mean $\log_2$-fold change analyzed by GSEA using GO biological process terms. Enrichment network visualized for gene sets with FDR < 0.01. Node sizes correspond to the number of genes in the GO term gene sets that also occur in the fold-change gene input list. Clusters of similar ontologies were manually assigned a group name based on high-level biological processes shared among nodes. **B,** Global profiling of splicing changes in response to pH in mouse and human dataset. Percent spliced (PSI = inclusion ratio/inclusion ratio + exclusion ratio) of all exons in normal pH (pH7.4) and acidic pH (pH6.4). **B′,** 298 orthologous exons (padj < 0.05, FDR < 0.01, and abs Δ PSI > 0.05) significantly spliced in mouse and human datasets (hypergeometric statistics, $P = 10^{-30}$). **B″,** GSEA of orthologous exons. **B‴,** GSEA of same list for identification of associated pathways.

Published OnlineFirst February 12, 2019; DOI: 10.1158/0008-5472.CAN-18-1604

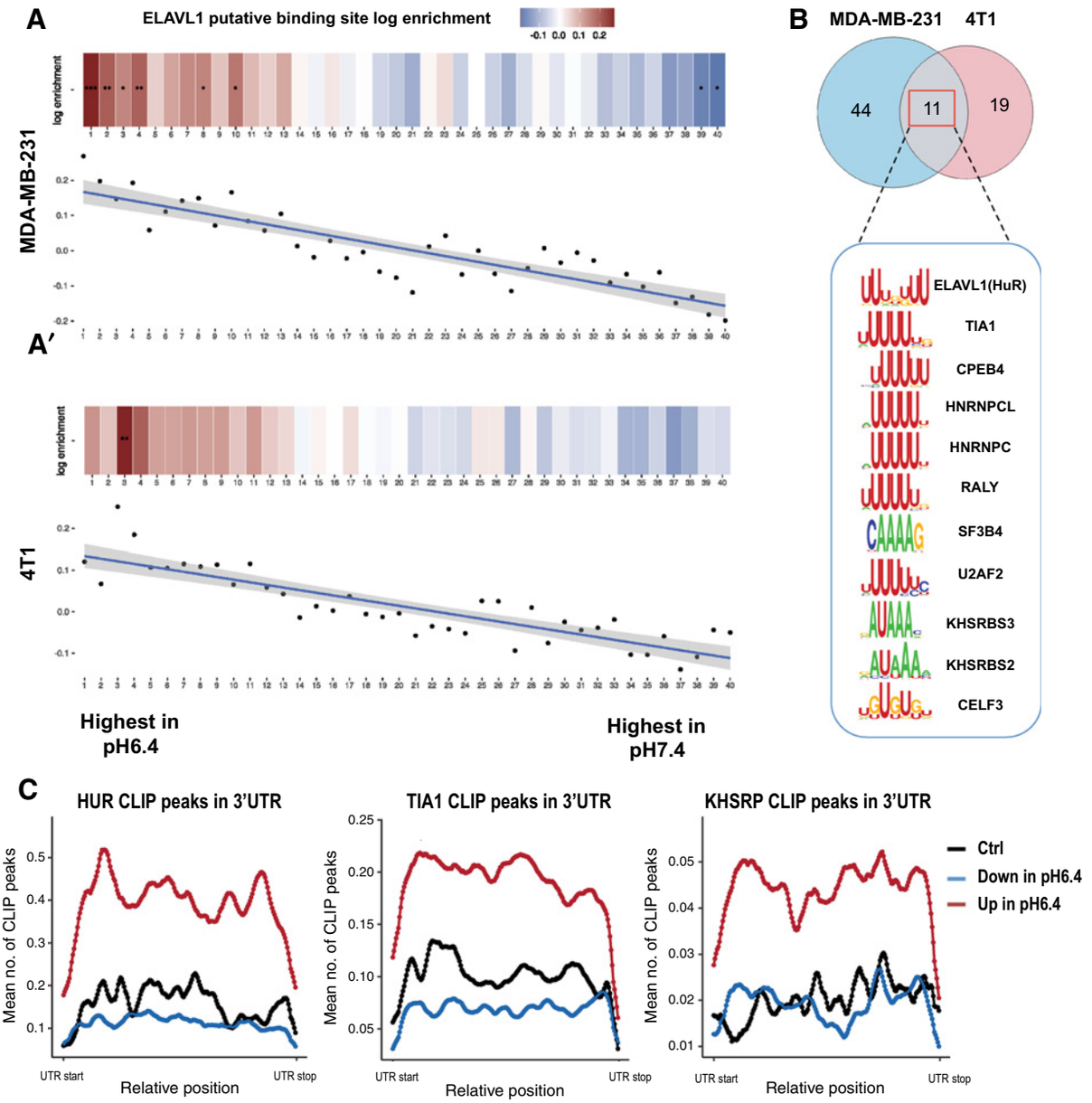

Figure 4.

Targets of RNA binding proteins with AU-rich motifs are enriched in genes upregulated in response to low pH. **A,** Spectrum plot generated by Transite suggests a highly nonrandom arrangement of putative binding sites across all transcripts. The transcripts from RNA-seq data set for MDA-MB-231 and 4T1 sorted by $\log_2$-fold change pH7.4/pH 6.4 in ascending order; transcripts with highest expression in low pH 6.4 (negative fold change) are on the left, downregulated transcripts on the right. Putative ELAVL1 binding sites are enriched in transcripts upregulated in low pH 6.4 (red) and depleted in transcripts downregulated (blue). **B,** Venn diagram depicts the overlap amongst the RBPs, with a significant overrepresentation of putative binding sites in transcripts upregulated in low pH conditions in human and mouse datasets. **C,** The enrichment of CLIP peaks for HUR, TIA1, and KHSRP at 3′UTR of transcripts upregulated in low pH indicate the binding sites of these RBPs are enriched in acidosis conditions. Metaplots of CLIP densities in 3′UTRs are plotted for genes up in low pH (>1.5-fold relative to control) down in pH 6, genes down in low pH (>1.5-fold relative to control), and control genes, where the fold-change in gene expression was less than 1.1-fold between both conditions. Significance of putative binding site enrichment values per bin indicated in spectrum plots as *, $P \leq 0.05$; **, $P \leq 0.01$; ***, $P \leq 0.001$).

4 hours, splicing of all three other candidates was significantly changed only after 48-hour exposure to low pH conditions (Supplementary Fig. S5A), at which point, cell growth remained equal to normal pH but, as expected, the growth rate was significantly reduced when assessed at the 96-hour time point (Supplementary Fig. S5B). Analysis of MDA-MB-231 cells cultured for 48 hours in acidic media and then returned to a normal pH medium for another 48 hours revealed that the splicing events were reversible and responsive to the extracellular pH alterations (Fig. 5A).

Published OnlineFirst February 12, 2019; DOI: 10.1158/0008-5472.CAN-18-1604

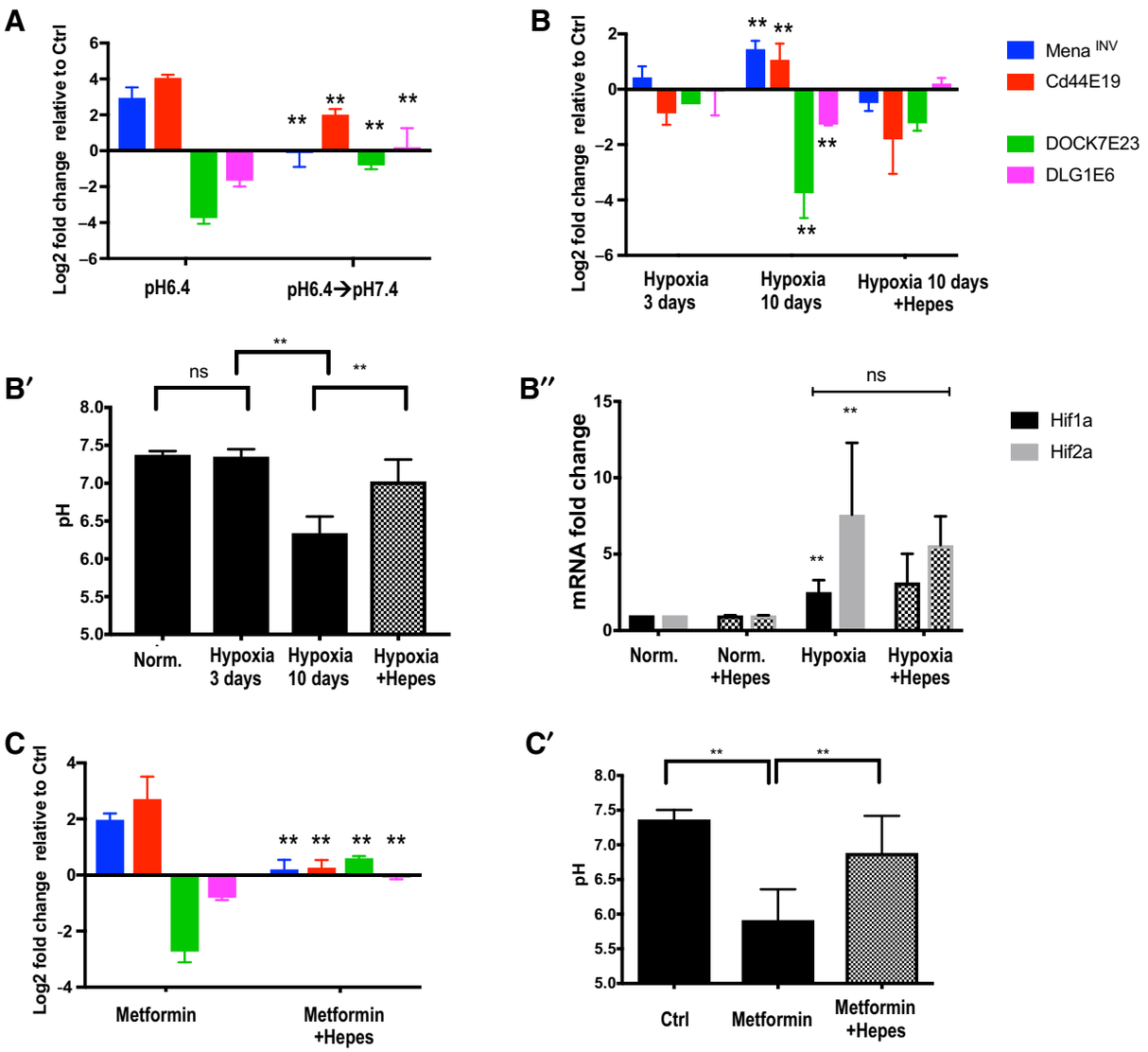

Figure 5.

Candidate splicing events are pH responsive. **A,** Inclusion/exclusion ratio relative fold change of candidate events 48 hours after exchange of low-pH medium with pH7.4 medium. **B,** Inclusion/exclusion ratio relative fold change of candidate events after culture in 0.2% oxygen ± 50 mmol/L HEPES. **B′,** pH of media in which cells were cultured for 3 days or 10 days in 0.2% oxygen ± HEPES. **B″,** Hif1 and Hif2 mRNA expression levels in hypoxic conditions ± 50 mmol/L HEPES. **C,** Inclusion/exclusion ratio fold change of candidate events following lactate acidosis induction by metformin ± HEPES addition. **C′,** pH of the culture medium following metformin treatment ± HEPES addition. $N = 4$ experiments, two technical replicates. Student t test, **, $P < 0.01$. ns, nonsignificant.

We next wondered whether the *in vivo* mechanisms underlying tumor acidosis, hypoxia, and aerobic glycolysis, could also trigger the same splicing events *in vitro*. Cells were subjected to hypoxic conditions for three or 10 days followed by RT-qPCR analysis. Although short-term hypoxia was insufficient for splicing of the candidates, long-term hypoxia induced changes similar to those observed under low pH conditions (Fig. 5B), coinciding with a drop in the pH of the medium to pH ∼6.3 after 10 days of hypoxia (Fig. 5B′). Thus, we hypothesized that the observed changes in splicing after 10 days of hypoxia were an indirect consequence of the reduced pH of the media (Fig. 5B). Consistent with this hypothesis, addition of HEPES to buffer the media blocked both the reduction in pH after 10 days of hypoxia and the resulting changes in splicing of the candidate genes (Fig. 5B–B′). Interestingly, buffering did not alter expression of two known transcriptional mediators of hypoxic effects, HIF1 and HIF2 (Fig. 5B″), suggesting that low pH-induced splicing events may arise independently of both HIF1 and HIF2 expression.

To mimic increased glycolysis conditions in culture, we used metformin, a drug that inhibits the complex I of mitochondria and therefore forces excessive lactate production (44). As expected, metformin addition increased the amount of lactate in the media and acidified the media (Fig. 5C′). Metformin addition also induced the pattern of low pH-induced splicing, which were

Published OnlineFirst February 12, 2019; DOI: 10.1158/0008-5472.CAN-18-1604

blocked by addition of HEPES (Fig. 5C). Lactate content remained increased under hypoxic or lactate acidosis conditions with or without HEPES buffering (Supplementary Fig. S5C and S5D). These results indicate that, at least for the splicing events tested, exposure to extracellular acidity is sufficient to induce the observed changes, while hypoxia-induced changes in HIF expression or increased lactate are dispensable.

The splicing of low pH-induced Mena^{INV} and of CD44E19 is sensitive to histone acetylation status

To explore the potential intracellular mechanisms underlying pH-dependent splicing, we asked if low pH-induced chromatin modifications, particularly global histone deacetylation could influence splicing of the candidate events. In response to extracellular pH drop, increased HDAC expression and activity antagonizes intracellular pH reduction through the enhanced release of acetate anions (15). Histone acetylation status influences the association of RNA splicing factors with nascent mRNA and thus modulates splicing (45). We used the HDAC inhibitor Trichostatin A (TSA) to increase histone acetylation levels and asked if the splicing events were sensitive to increased histone acetylation levels. Interestingly TSA inhibited the pH-induced expression of CD44 E19 and Mena^{INV} but it did not influence the exclusions of DOCK7 E23 and DLG1 E6 (Supplementary Fig. S5E and S5F). Thus, we conclude that the pH-induced inclusion of CD44 E19 and Mena^{INV} is sensitive to histone acetylation status, suggesting a role for pH-induced chromatin deacetylation in the modulation of some of the RNA splicing changes observed in low pH signature.

The low pH-induced transcriptomic signature *in vivo*

We next asked whether the pH-responsive gene signature could be observed in cells exposed to tumor acidosis *in vivo*. We used the pHLIP-Cy7 peptide to label cells in low-pH tumor areas and then used FACS of disaggregated tumor cells to recover cells retaining the peptide (Fig. 6A). The Cy7-positive and -negative cell populations representing cells from acidic and nonacidic tumor regions, respectively, were then evaluated for candidate gene expression and exon usage by RT-qPCR. The expression of all genes in the cells collected from PyMT mouse tumors followed a pattern similar to that observed in low-pH conditions *in vitro* (Fig. 6B; Supplementary Fig. S6A).

Next, we tested if the spatial expression of candidate pH-responsive spliced isoforms correlated with the acidic areas of the tumor using ISH and immunofluorescence. An existing antibody specific to the Mena isoform containing the pH-responsive exon inclusion (Mena^{INV}; ref. 21) was used to evaluate the expression of this isoform relative to acidic tumor areas. Most Mena^{INV}-positive cells were also pHLIP-positive, both in primary tumors and in the metastatic lesions (Fig. 6C–E). Furthermore, cells expressing highest Mena^{INV} levels were located closest to the tumor–stroma interface (Fig. 6D–F). Similarly, human IDC tumors exhibited a significant overlap between Mena^{INV} expression and CA9 (Supplementary Fig. S6B) with Mena^{INV} positive cells enriched at the tumor–stroma interface (Supplementary Fig. S6C). To detect the expression of CD44 E19 in human tumor sections we used an ISH approach with an RNAscope probe specific to E19. Most CD44 E19-positive cells overlapped with the expression of CA9 in the patient tumors examined (Supplementary Fig. S6D) and were present at the peripheral tumor regions marked by CA9 expression (Supplementary Fig. S6E). These data confirmed that the expression of at least a subset of candidate pH-responsive splicing events correlates with areas marked either by pHLIP retention at the membrane or CA9 expression.

Given the association of acidosis *in vitro* with increased histone deacetylation and the influence on the expression of Mena^{INV} and CD44 E19, we asked if the expression of HDACs *in vivo* also correlates with the acidic areas. Using an antibody against HDAC2 we evaluated its expression relative to acidic regions. Interestingly, areas marked by pHLIP in mouse expressed high levels of HDAC (Fig. 6G). These high-expressing HDAC cells were frequently enriched at tumor–stroma interfaces (Fig. 6H). This observation suggests a potential molecular explanation for previously reported pH-Induced global histone deacetylation (15). Altogether, these findings indicate that acidic areas *in vivo* are sites of increased HDAC expression, which in turn, influence the expression of pH-induced splicing events such as Mena^{INV} and CD44E19.

Tumor neutralization abrogates the expression of pH-responsive isoforms

To evaluate the pH responsiveness of the candidate splicing events *in vivo*, we examined the events in tumors collected from mice that received regular or bicarbonate water. As before, consumption of bicarbonate water was sufficient to reduce tumor acidity, evident by the reduction of pHLIP-localization in cells from those tumors relative to control (Fig. 7A–A′), and to reduce lung metastasis (26). In addition, the percentage of Mena^{INV} positive cells was significantly reduced in those tumors (Fig. 7A′–A″). To examine the pH-responsive splicing candidates *in vivo*, tumors from control or treated mice were analyzed by qPCR analysis. Compared with the control samples, in tumors from PyMT mice that consumed bicarbonate water the inclusion ratio of the INV exon of Mena was significantly reduced. Similarly, the DOCK7 exon 23 and DLG1 exon 6 trended toward increased ratios, following the expected directionality, however, in these cases the changes were not statistically significant (Fig. 7B). The effect of buffering on pH-responsive exons was also evaluated in a xenograft model derived from MDA-MB-231 cells. In line with the findings in the MMTV-PyMT tumors, the appearance of all candidate pH-responsive splicing events was significantly attenuated in tumors collected from bicarbonate water treated group in the xenograft model (Fig. 7C). These data indicate that alteration in the extracellular acidity *in vivo* directly influences the expression of the pH-responsive signature.

Discussion

We characterized the spatial characteristics of acidic tumor microenvironment using pHLIP technology, and demonstrated that tumor–stroma interfaces are acidic and that cells within the acidic front are invasive and proliferative. We found that exposure to low extracellular pH *in vitro* modulates RNA metabolism, particularly RNA splicing, and identified a potential role for a family of RBPs with affinity for AU-rich motif, in the pH-induced transcriptomic signature. The low-pH signature indicated extensive changes in alternative splicing and was notably enriched for splicing of genes implicated in regulation of adhesion and cell migration. Although the global regulation of RNA splicing in response to acidosis *in vivo* remains to be determined, we demonstrated that a set of functionally important candidate splicing

Published OnlineFirst February 12, 2019; DOI: 10.1158/0008-5472.CAN-18-1604

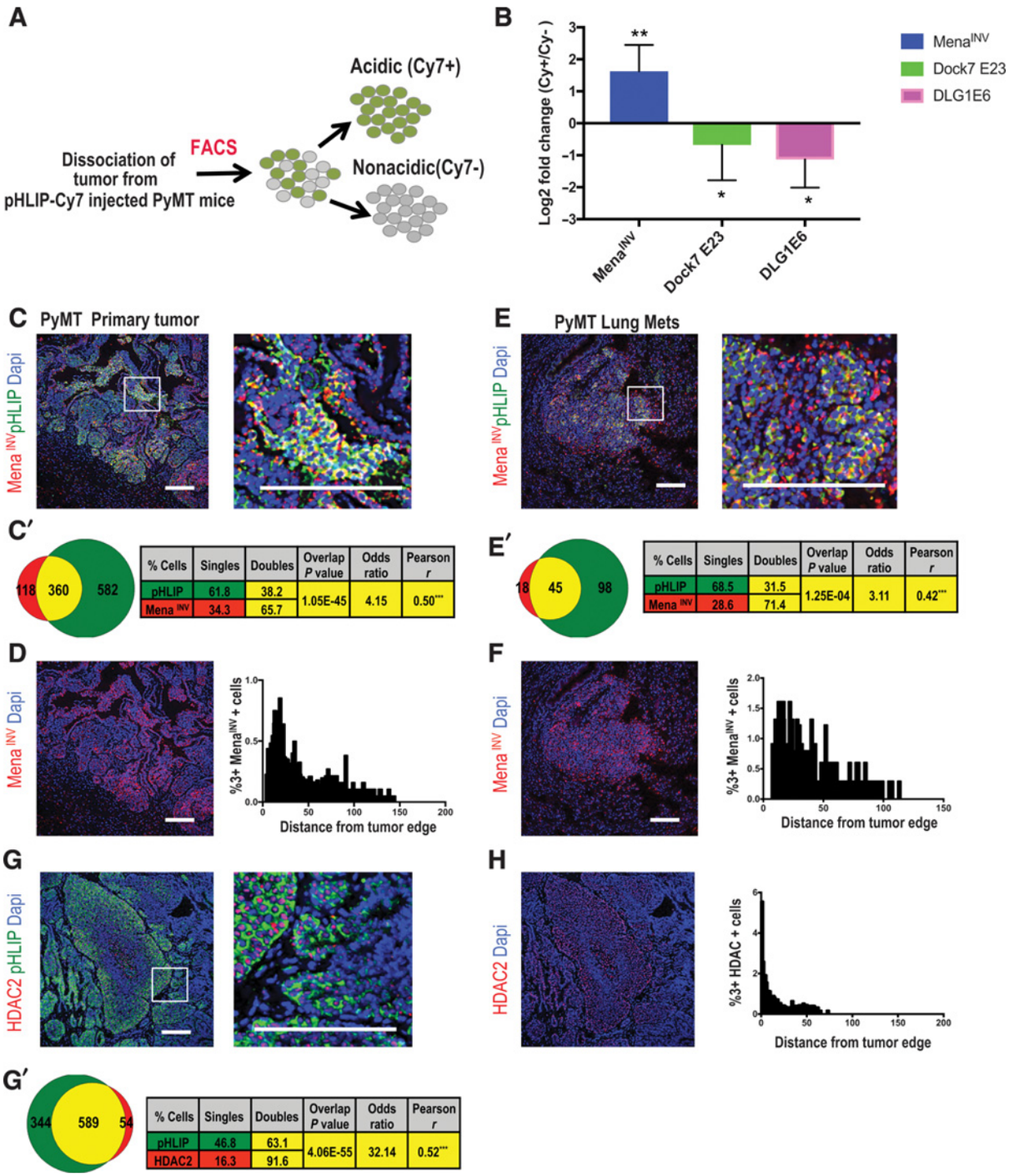

Figure 6.

In vivo validation of pH-responsive transcriptomic changes. **A,** Schematic of workflow for isolating cells from the low pH tumor areas. **B,** Inclusion/exclusion ratio relative fold change of candidate events in sorted pHLIP-positive vs. pHLIP-negative cells. **C** and **E,** Expression and colocalization analysis of Mena^{INV} immunofluorescence relative to pHLIP-labeled acidic areas in primary and metastatic lesions from PyMT mice. **C′** and **E′,** Cell-based overlap and Pearson correlation coefficient analysis of Mena^{INV} and pHLIP-positive cells. **D** and **F,** Spatial distribution of Mena^{INV} (3+)-expressing cells relative to tumor–stroma interfaces in primary tumor and metastatic lesions. **G,** Immunofluorence of HDAC2 and pHLIP in PyMT tumor. **G′,** Cell-based overlap and Pearson correlation coefficient of HDAC2 and pHLIP. **H,** Spatial distribution of HDAC (3+) expressing cells relative to tumor–stroma interface in primary tumor. $N = 5$ experiments, two technical replicates. Students t test, *, $P < 0.05$; **, $P < 0.01$; ***, $P \leq 0.001$. Scale bars, 100 μm.

Published OnlineFirst February 12, 2019; DOI: 10.1158/0008-5472.CAN-18-1604

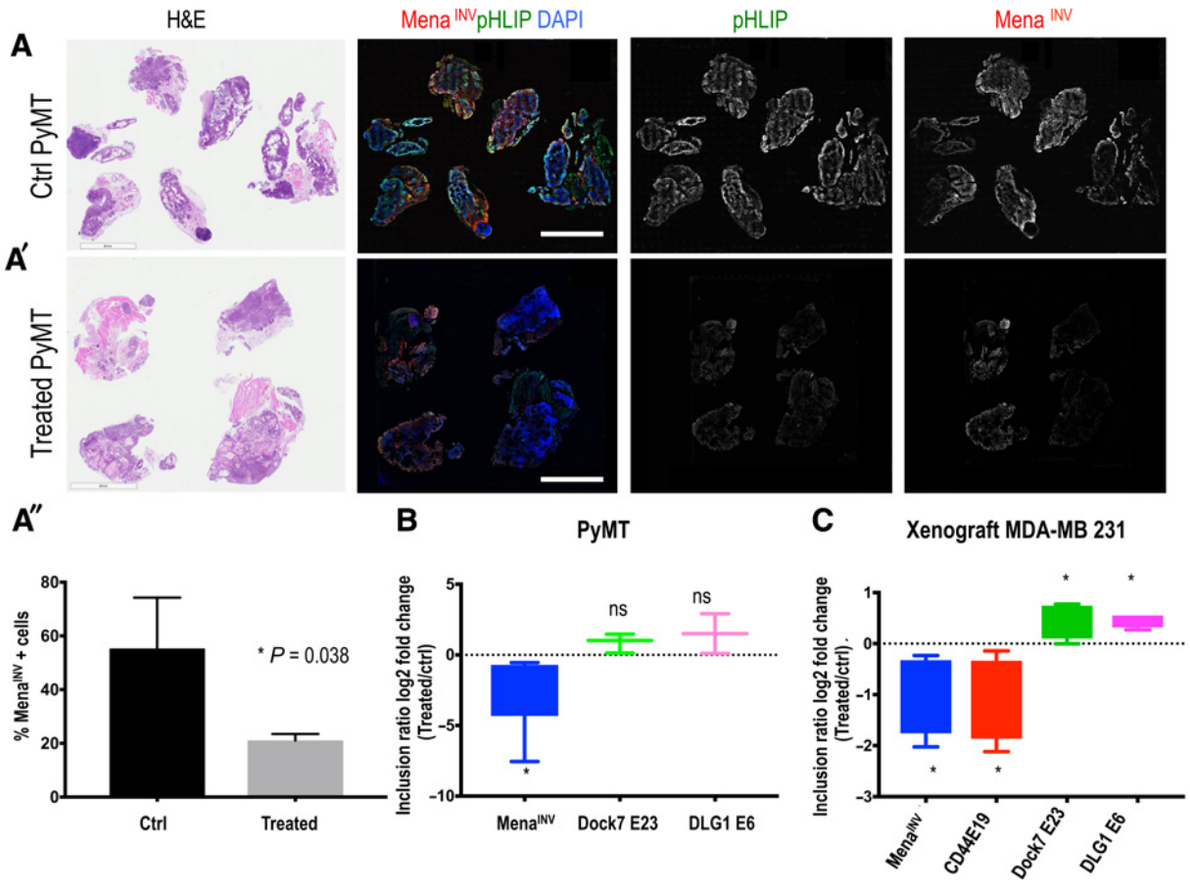

Figure 7.

Buffering tumor acidity significantly modulates the expression of candidate splicing events. **A–A′,** Immunofluorescence of Mena^{INV} isoform and pHLIP in control or alkalinized tumors collected from PyMT mice ($n = 7$ per group). Scale bar, 4 mm. **A″,** Percentages of total Mena^{INV}-positive cells measured by immunostaining. H&E, hematoxylin and eosin. **B** and **C,** qPCR analysis on bulk tumors collected from control and bicarbonated water–treated MMTV-PyMT and xenograft tumor from NOD SCID mice. *, $P < 0.05$; ns, nonsignificant.

events is similarly pH responsive *in vitro* and *in vivo*. The pH-responsive splicing of Mena and CD44 was sensitive to pH-induced histone deacetylation *in vitro,* demonstrating a link between chromatin deacetylation and modulation of RNA splicing in response to extracellular acidity. These findings provide new molecular insight into one way in which acidosis contributes to local transcriptomic alterations that promote prometastatic phenotypes.

Consistent with its well established role in local invasion and malignant progression (7, 46), we found that acidosis is enriched adjacent to tumor–stroma interfaces in addition to areas within hypoxic cores. Acidosis in well-oxygenated areas can be caused by adaptation to increased aerobic glycolysis or oxidative phosphorylation (1, 47). LDHA expression was indeed enriched within a subset of acidic cellular areas at the tumor–stroma interfaces (3, 32). Acidic regions, however, were not restricted to sites of increased glycolysis marked by LDHA, indicating that acidosis may also be induced by other means such as protons generated through oxidative phosphorylation. Prolonged exposure to extracellular acidification shifts cancer cell metabolic reprogramming towards reactive oxygen species homeostasis and therefore promotes proliferation and aggressive phenotypes under harsh conditions. An example of such mechanism is mediated through a balance between histone deacetylation, mitochondrial hyper acetylation, and increased fatty acid oxidation (16). Consistently, we observed that cells within low pH areas express high levels of HDAC and Ki-67 *in vivo*. Our results build upon previous reports on the correlation of extracellular acidity and local growth (7) and improve our understanding of the distribution of the acidic microenvironment relative to hallmarks of tumor progression.

The global functional consequences of the acidosis-induced splicing program largely remain to be determined but, for example, inclusion of the INV exon of Mena plays important roles in promoting directional migration, ECM remodeling, stabilization of invadopodia and metastasis. In addition, the Mena^{INV} isoform is associated with poor clinical outcome of breast cancer patients (48). The inclusion of exon 19 of CD44 generates a short isoform of CD44 with a truncated cytoplasmic tail. Its expression *in vitro* is upregulated in multidrug-resistant MCF-7/Adr cells, and also affects cell invasion through the Ras/MAPK signaling pathway (37). Here we demonstrate both *in vivo* and *in vitro* that acidosis is necessary and sufficient to drive the expression of these isoforms in both mouse and human tumors. These examples indicate that acidic microenvironment induces the expression of

isoforms of genes associated with malignancy; however, it remains to be established if acidosis *in vivo* induces a global transcriptomic rewiring that influences splicing similar to the phenomenon observed *in vitro*.

The mechanisms underlying acidosis-dependent changes in RNA metabolism and splicing are unknown. Cellular stress responses involving the formation of ribonucleoprotein complexes and stress granules that impact RNA splicing, RNA stability, and posttranscriptional regulation have been proposed (49). Furthermore, adaptive mechanisms that influence protein synthesis and half-life may affect the abundance of specific RNA binding proteins and thus impact regulation of RNA splicing in response to acidic stress (14). Whether adaptive pathways that maintain physiologic internal pH_i in response to low extracellular pH affect these mechanisms, and if these mechanisms contribute to pH-dependent transcriptomic changes are important questions for future studies. The pH-induced global histone deacetylation is an example of such homeostatic mechanism that contributes to maintenance of internal pH (15, 50). We found that pH-induced acetylation status influences some of the pH-dependent splicing changes we observed, including the inclusions of CD44E19 and of $Mena^{INV}$, further suggesting that the transcriptomic changes including alternative splicing may be coordinated with adaptive intracellular mechanisms that transduce pH_e alterations. Acetylation of histones could directly influence the interaction of RNA splicing factors with nascent mRNA and thus affect alternative splicing (45). Alternatively, histone acetylation can influence RNA polymerase processivity, which in turn modulates the splicing of alternative exons (51). Interestingly, the ELAVL/HUR family, whose targets were highly enriched in the pH-induced signature in this study, affects RNA splicing through a similar mechanism. HUR modulates RNA splicing indirectly by inducing localized histone hyper-acetylation through inhibition of HDAC2. Local histone hyper-acetylation leads to increased transcriptional elongation, which promotes skipping of HUR target sites and therefore favors inclusion of constitutive exons (52). We speculate that in low pH conditions HUR also influences global splicing rewiring, which involves downregulation of constitutive exons and splicing-in of alternatively included exons. In addition to regulating splicing, HUR has a well-established role in stabilizing target mRNAs. Therefore, the observed increase in HUR targets in the low pH signature may reflect two aspects of HUR function: (i) a reduced ability of HUR to suppress inclusions of target alternatively included exons by hyper-acetylation and (ii) increased stabilization of mRNAs containing its binding site. This is consistent with the observed global transcriptomic rewiring and the enrichment of the HUR targets in the 3′UTR of transcripts up regulated in response to low pH.

Together, our results lead us to propose that acidosis, an intrinsic feature of the microenvironment, is enriched at the tumor invasive fronts and triggers adaptive changes in gene expression and splicing that are potentially controlled through a specific set of RBPs and downstream of pH-induced chromatin modifications. Our study provides new insights into how acidosis contributes to alterations underlying malignant progression. Understanding how acidosis evokes transcriptomic changes that confer aggressive tumor phenotypes will provide therapeutically valuable insight.

Disclosure of Potential Conflicts of Interest

No potential conflicts of interest were disclosed.

Authors' Contributions

Conception and design: N. Rohani, M.N. Moufarrej, D.A. Lauffenburger, S.N. Bhatia, F.B. Gertler

Development of methodology: N. Rohani, M.N. Moufarrej, M.B. Yaffe

Acquisition of data (provided animals, acquired and managed patients, provided facilities, etc.): N. Rohani, L. Hao, M.N. Moufarrej

Analysis and interpretation of data (e.g., statistical analysis, biostatistics, computational analysis): N. Rohani, M.S. Alexis, B.A. Joughin, K. Krismer, M.N. Moufarrej, A.R. Soltis, M.B. Yaffe, C.B. Burge

Writing, review, and/or revision of the manuscript: N. Rohani, L. Hao, B.A. Joughin, M.N. Moufarrej, D.A. Lauffenburger, M.B. Yaffe, S.N. Bhatia, F.B. Gertler

Administrative, technical, or material support (i.e., reporting or organizing data, constructing databases): N. Rohani, L. Hao, F.B. Gertler

Study supervision: N. Rohani, D.A. Lauffenburger, S.N. Bhatia, F.B. Gertler

Acknowledgments

We thank Gertler lab members for helpful discussions and technical assistance; Robert Weinberg and Matthew Vander Heiden for support and helpful discussions; John Lamar, Daniel Stover, and Lucas Sullivan for reagents; Simon Gordonov for MATLAB scripts used in the generation of figures; Shannon Hughes for critical reading of the manuscript; and the KI Swanson Biotechnology Center, Duanduan Ma and Stuart S. Levine (Bioinformatics core), Eliza Vasile (Microscopy Core Facility), and Kathleen Cormier (Histology Facility) for technical support. This work was supported by KI NCI Core Grant P30-CA14051; U54-CA112967 to D.A. Lauffenburger and F.B. Gertler; HHMI 1122028 to S.N. Bhatia; NIH R01-GM069668 to D.A. Lauffenburger; U01-CA184897 to F.B. Gertler and C.B. Burge; R01-ES015339 and R35-ES028374 to M.B. Yaffe; and NIH grant P30-CA14051 to M.B. Yaffe and C.B. Burge. N. Rohani and L. Hao were supported by KI Quinquennial Cancer Research Fellowship. M.N. Moufarrej was supported through MIT's Undergraduate Research Opportunities Program.

The costs of publication of this article were defrayed in part by the payment of page charges. This article must therefore be hereby marked *advertisement* in accordance with 18 U.S.C. Section 1734 solely to indicate this fact.

Received May 25, 2018; revised September 19, 2018; accepted February 6, 2019; published first February 12, 2019.

References

1. Gatenby RA, Smallbone K, Maini PK, Rose F, Averill J, Nagle RB, et al. Cellular adaptations to hypoxia and acidosis during somatic evolution of breast cancer. Br J Cancer 2007;97:646–53.
2. Damaghi M, Tafreshi NK, Lloyd MC, Sprung R, Estrella V, Wojtkowiak JW, et al. Chronic acidosis in the tumour microenvironment selects for overexpression of LAMP2 in the plasma membrane. Nat Commun 2015;6:8752. doi: 10.1038/ncomms9752.
3. Robertson-Tessi M, Gillies RJ, Gatenby RA, Anderson AR. Impact of metabolic heterogeneity on tumor growth, invasion, and treatment outcomes. Cancer Res 2015;75:1567–79.
4. Andreucci E, Peppicelli S, Carta F, Brisotto G, Biscontin E, Ruzzolini J, et al. Carbonic anhydrase IX inhibition affects viability of cancer cells adapted to extracellular acidosis. J Mol Med 2017;95:1341–53.
5. Wojtkowiak JW, Verduzco D, Schramm KJ, Gillies RJ. Drug resistance and cellular adaptation to tumor acidic pH microenvironment. Mol Pharm 2011;8:2032–8.
6. Lloyd MC, Cunningham JJ, Bui MM, Gillies RJ, Brown JS, Gatenby RA. Darwinian dynamics of intratumoral heterogeneity: not solely random mutations but also variable environmental selection forces. Cancer Res 2016;76:3136–44.

Published OnlineFirst February 12, 2019; DOI: 10.1158/0008-5472.CAN-18-1604

7. Estrella V, Chen T, Lloyd M, Wojtkowiak J, Cornnell HH, Ibrahim-Hashim A, et al. Acidity generated by the tumor microenvironment drives local invasion. Cancer Res 2013;73:1524–35.
8. Huber V, Camisaschi C, Berzi A, Ferro S, Lugini L, Triulzi T, et al. Cancer acidity: an ultimate frontier of tumor immune escape and a novel target of immunomodulation. Semin Cancer Biol 2017;43:74–89.
9. Lin Y, Chang G, Wang J, Jin W, Wang L, Li H, et al. NHE1 mediates MDA-MB-231 cells invasion through the regulation of MT1-MMP. Exp Cell Res 2011;317:2031–40.
10. Magalhaes MAO, Larson DR, Mader CC, Bravo-Cordero JJ, Gil-Henn H, Oser M, et al. Cortactin phosphorylation regulates cell invasion through a pH-dependent pathway. J Cell Biol 2011;195:903–20.
11. Choi CH, Webb BA, Chimenti MS, Jacobson MP, Barber DL. Ph sensing by FAK-His58 regulates focal adhesion remodeling. J Cell Biol 2013;202: 849–59.
12. Han J, Li J, Ho JC, Chia GS, Kato H, Jha S, et al. Hypoxia is a key driver of alternative splicing in human breast cancer cells. Sci Rep 2017;7:1–17.
13. Chen JL, Lucas JE, Schroeder T, Mori S, Wu J, Nevins J, et al. The genomic analysis of lactic acidosis and acidosis response in human cancers. PLoS Genet 2008;4:e1000293.
14. Walton ZE, Patel CH, Brooks RC, Yu Y, Ibrahim-Hashim A, Riddle M, et al. Acid suspends the circadian clock in hypoxia through inhibition of mTOR. Cell 2018;174:72–87.e32.
15. McBrian MA, Behbahan IS, Ferrari R, Su T, Huang TW, Li K, et al. Histone acetylation regulates intracellular pH. Mol Cell 2013;49:310–21.
16. Corbet C, Pinto A, Martherus R, Santiago de Jesus JP, Polet F, Feron O. Acidosis drives the reprogramming of fatty acid metabolism in cancer cells through changes in mitochondrial and histone acetylation. Cell Metab 2016;24:311–23.
17. Helmlinger G, Yuan F, Dellian M, Jain RK. Interstitial pH and pO2 gradients in solid tumors in vivo: high-resolution measurements reveal a lack of correlation. Nat Med 1997;3:177–82.
18. Ma F, Li H, Wang H, Shi X, Fan Y, Ding X, et al. Enriched $CD44^{+}/CD24^{-}$ population drives the aggressive phenotypes presented in triple-negative breast cancer (TNBC). Cancer Lett 2014;353:153–9.
19. Andreev OA, Karabadzhak AG, Weerakkody D, Andreev GO, Engelman DM, Reshetnyak YK. pH (low) insertion peptide (pHLIP) inserts across a lipid bilayer as a helix and exits by a different path. Proc Natl Acad Sci U S A 2010;107:4081–6.
20. Adochite RC, Moshnikova A, Carlin SD, Guerrieri RA, Andreev OA, Lewis JS, et al. Targeting breast tumors with pH (Low) insertion peptides. Mol Pharm 2014;11:2896–905.
21. Oudin M, Hughes S, Rohani N, Moufarrej M, Jones J, Condeelis J, et al. Characterization of the expression of the pro-metastatic MenaINV isoform during breast tumor progression. Clin Exp Metastasis 2015;1–13.
22. Subramanian A, Tamayo P, Mootha VK, Mukherjee S, Ebert BL, Gillette MA, et al. Gene set enrichment analysis: a knowledge-based approach for interpreting genome-wide expression profiles. Proc Natl Acad Sci U S A 2005;102:15545–50.
23. Krismer K, Varmeh S, Bird MA, Gattinger A, Kong YW, Bernwinkler T, et al. Transite: a computational motif-based analysis platform that identifies RNA-binding proteins modulating changes in gene expression. bioRxiv 2018. doi: https://doi.org/10.1101/416743.
24. Van Nostrand EL, Freese P, Pratt GA, Wang X, Wei X, Blue SM, et al. A large-scale binding and functional map of human RNA binding proteins. bioRxiv 2017. doi: https://doi.org/10.1101/179648.
25. Lebedeva S, Jens M, Theil K, Schwanhäusser B, Selbach M, Landthaler M, et al. Transcriptome-wide analysis of regulatory interactions of the RNA-binding protein HuR. Mol Cell 2011;43:340–52.
26. Robey IF, Baggett BK, Kirkpatrick ND, Roe DJ, Dosescu J, Sloane BF, et al. Bicarbonate increases tumor pH and inhibits spontaneous metastases. Cancer Res 2009;69:2260–8.
27. Robey IF, Nesbit LA. Investigating mechanisms of alkalinization for reducing primary breast tumor invasion. Biomed Res Int 2013;2013:485196. doi: 10.1155/2013/485196.
28. Weerakkody D, Moshnikova A, Thakur MS, Moshnikova V, Daniels J, Engelman DM, et al. Family of pH (low) insertion peptides for tumor targeting. Proc Natl Acad Sci U S A 2013;110:5834–9.
29. Swietach P, Vaughan-Jones RD, Harris AL. Regulation of tumor pH and the role of carbonic anhydrase 9. Cancer Metastasis Rev 2007;26:299–310.
30. Lee SH, McIntyre D, Honess D, Hulikova A, Pacheco-Torres J, Cerdán S, et al. Carbonic anhydrase IX is a pH-stat that sets an acidic tumour extracellular pH in vivo. Br J Cancer 2018;119:622–30.
31. Dovmark TH, Saccomano M, Hulikova A, Alves F, Swietach P. Connexin-43 channels are a pathway for discharging lactate from glycolytic pancreatic ductal adenocarcinoma cells. Oncogene 2017;36:4538–50.
32. Valvona CJ, Fillmore HL, Nunn PB, Pilkington GJ. The regulation and function of lactate dehydrogenase a: therapeutic potential in brain tumor. Brain Pathol 2016;26:3–17.
33. Panisova E, Kery M, Sedlakova O, Brisson L, Debreova M, Sboarina M, et al. Lactate stimulates CA IX expression in normoxic cancer cells. Oncotarget 2017;8:77819–35.
34. Brisson L, Reshkin SJ, Goré J, Roger S. PH regulators in invadosomal functioning: proton delivery for matrix tasting. Eur J Cell Biol 2012;91: 847–60.
35. Paradise RK, Whitfield MJ, Lauffenburger DA, Van Vliet KJ. Directional cell migration in an extracellular pH gradient: a model study with an engineered cell line and primary microvascular endothelial cells. Exp Cell Res 2013;319:487–97.
36. Zhao W, Zhao J, Hou M, Wang Y, Zhang Y, Zhao X, et al. HuR and TIA1/TIAL1 are involved in regulation of alternative splicing of SIRT1 pre-mRNA. Int J Mol Sci 2014;15:2946–58.
37. Fang XJ, Jiang H, Zhu YQ, Zhang LY, Fan QH, Tian Y. Doxorubicin induces drug resistance and expression of the novel CD44st via NF-κB in human breast cancer MCF-7 cells. Oncol Rep 2014;31:2735–42.
38. Jiang H, Knudson CB, Knudson W. Antisense inhibition of CD44 tailless splice variant in human articular chondrocytes promotes hyaluronan internalization. Arthritis Rheum 2001;44:2599–610.
39. Philippar U, Roussos ET, Oser M, Yamaguchi H, Kim HD, Giampieri S, et al. A Mena invasion isoform potentiates EGF-induced carcinoma cell invasion and metastasis. Dev Cell 2008;15:813–28.
40. Roussos ET, Balsamo M, Alford SK, Wyckoff JB, Gligorijevic B, Wang Y, et al. Mena invasive (MenaINV) promotes multicellular streaming motility and transendothelial migration in a mouse model of breast cancer. J Cell Sci 2011;124:2120–31.
41. Murray DW, Didier S, Chan A, Paulino V, Van Aelst L, Ruggieri R, et al. Guanine nucleotide exchange factor Dock7 mediates HGF-induced glioblastoma cell invasion via Rac activation. Br J Cancer 2014;110:1307–15.
42. Sandoval GJ, Graham DB, Gmyrek GB, Akilesh HM, Fujikawa K, Sammut B, et al. Novel mechanism of tumor suppression by polarity gene discs large 1 (DLG1) revealed in a murine model of pediatric B-ALL. Cancer Immunol Res 2013;1:426–37.
43. Tam WL, Lu H, Buikhuisen J, Soh BS, Lim E, Reinhardt F, et al. Protein kinase C α is a central signaling node and therapeutic target for breast cancer stem cells. Cancer Cell 2013;24:347–64.
44. Andrzejewski S, Gravel SP, Pollak M, St-Pierre J. Metformin directly acts on mitochondria to alter cellular bioenergetics. Cancer Metab 2014;2:12. doi: 10.1186/2049-3002-2-12.
45. Hnilicová J, Hozeifi S, Dušková E, Icha J, Tománková T, Staněk D. Histone deacetylase activity modulates alternative splicing. PLoS One 2011;6: e16727. doi: 10.1371/journal.pone.0016727.
46. Webb BA, Chimenti M, Jacobson MP, Barber DL. Dysregulated pH: a perfect storm for cancer progression. Nat Rev Cancer 2011;11:671–7.
47. Gillies RJ, Gatenby RA. Adaptive landscapes and emergent phenotypes: why do cancers have high glycolysis? J Bioenerg Biomembr 2007;39: 251–7.
48. Gertler F, Condeelis J. Metastasis: tumor cells becoming MENAcing. Trends Cell Biol 2011;21:81–90.
49. David CJ, Manley JL. Alternative pre-mRNA splicing regulation in cancer: pathways and programs unhinged. Genes Dev 2010;24:2343–64.
50. Corbet C, Draoui N, Polet F, Pinto A, Drozak X, Riant O, et al. The SIRT1/HIF2α axis drives reductive glutamine metabolism under chronic acidosis and alters tumor response to therapy. Cancer Res 2014;74:5507–19.
51. Zhou HL, Luo G, Wise JA, Lou H. Regulation of alternative splicing by local histone modifications: potential roles for RNA-guided mechanisms. Nucleic Acids Res 2014;42:701–13.
52. Zhou HL, Hinman MN, Barron VA, Geng C, Zhou G, Luo G, et al. Hu proteins regulate alternative splicing by inducing localized histone hyperacetylation in an RNA-dependent manner. Proc Natl Acad Sci U S A 2011; 108:E627–35.

Published OnlineFirst February 12, 2019; DOI: 10.1158/0008-5472.CAN-18-1604

Cancer Research
The Journal of Cancer Research (1916–1930) | The American Journal of Cancer (1931–1940)

AACR American Association for Cancer Research

Acidification of Tumor at Stromal Boundaries Drives Transcriptome Alterations Associated with Aggressive Phenotypes

Nazanin Rohani, Liangliang Hao, Maria S. Alexis, et al.

Cancer Res 2019;79:1952-1966. Published OnlineFirst February 12, 2019.